nature photonics

SUPPLEMENTARY INFORMATION

https://doi.org/10.1038/s41566-019-0373-y

In the format provided by the authors and unedited.

Self-stabilizing photonic levitation and propulsion of nanostructured macroscopic objects

Ognjen Ilic and Harry A. Atwater*

Department of Applied Physics and Materials Science, California Institute of Technology, Pasadena, CA, USA. *e-mail: haa@caltech.edu

nature photonics

SUPPLEMENTARY INFORMATION

https://doi.org/10.1038/s41566-019-0373-y

In the format provided by the authors and unedited.

Self-stabilizing photonic levitation and propulsion of nanostructured macroscopic objects

Ognjen Ilic and Harry A. Atwater*

Department of Applied Physics and Materials Science, California Institute of Technology, Pasadena, CA, USA. *e-mail: haa@caltech.edu

Supporting Information: Self-Stabilizing Photonic Levitation and Propulsion of Nanostructured Macroscopic Objects

Ognjen Ilic[1] and Harry A. Atwater[1]

[1]*Department of Applied Physics and Materials Science, California Institute of Technology, Pasadena, CA 91125, USA*

I. VISUALIZING SIMULATED DYNAMICS (FIG. 3B, VIDEO)

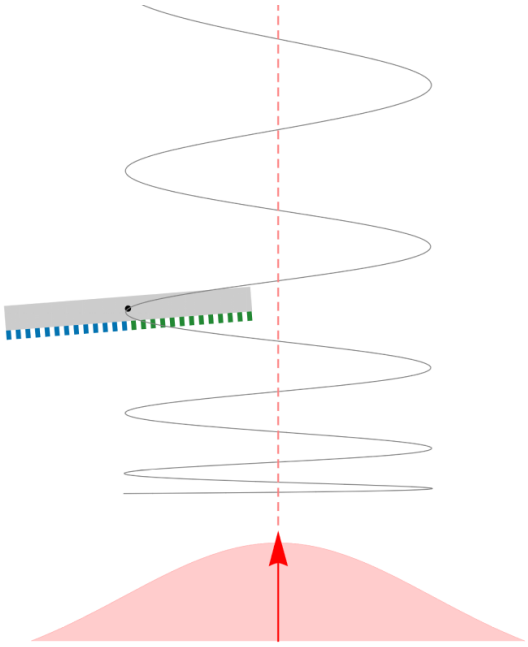

FIG. S1. Snapshot of the simulated dynamics from Fig. 3b of the main text. For the animation, see the included video 1.

II. LIGHT-INDUCED FORCE AND TORQUE ON A STRUCTURE WITH A UNIT CELL

We consider an electromagnetic wave impinging on a structure with a unit cell in the x-y plane, as shown in Fig. S2. The contribution to the total force and torque from the elements enclosed by the highlighted surface S can be expressed as [1]

$$\boldsymbol{F} = \int_{\partial S} (\mathbf{T} \cdot \hat{n}) dA, \qquad \boldsymbol{Q} = \int_{\partial S} r \times (\mathbf{T} \cdot \hat{n})\, dA$$

where the stress tensor is defined as $T_{ij} = \epsilon_0 \left(E_i E_j - \frac{1}{2} |\mathbf{E}|^2 \delta_{ij} \right) + \frac{1}{\mu_0} \left(B_i B_j - \frac{1}{2} |\mathbf{B}|^2 \delta_{ij} \right)$, and $\hat{n}$ is the unit vector normal to the surface. We assume that the lateral (x-y) extent of the structure is much greater than its transverse (z) extent, such that the dominant contribution to the stress tensor comes from the two faces of the integrating box parallel to the x-y plane.

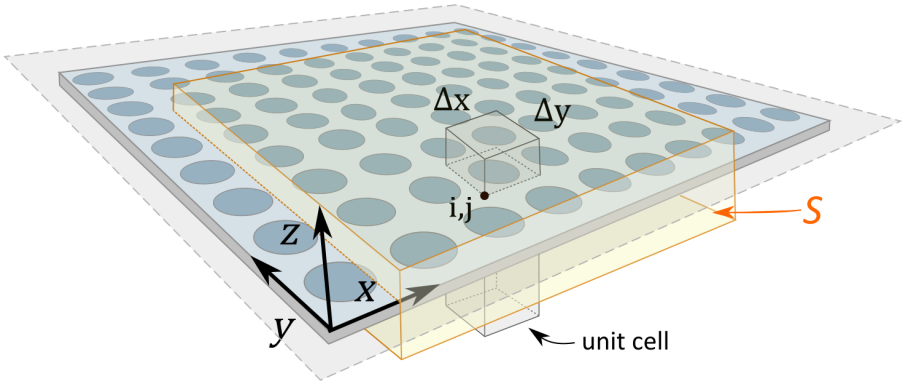

FIG. S2. Schematic of a portion of a large (e.g. macroscopic) structure that has a locally repeating unit cell.

For the force, we proceed to write

$$\begin{aligned}\boldsymbol{F} &= \int_{\partial S} \mathrm{d}x\mathrm{d}y \mathbf{T}(x,y)\cdot\hat{n} \\ &= \sum_{i,j}\int_{(i-1)\Delta x}^{i\Delta x}\mathrm{d}x\int_{(j-1)\Delta y}^{j\Delta y}\mathrm{d}y \mathbf{T}(x,y)\cdot\hat{n}\end{aligned}$$

where we decompose the surface integral over the sum of the unit cell integrals (as depicted in Fig. S2). We assume the beam width is much larger than the unit cell (of size $\Delta x \times \Delta y$, at position i, j). Expressing $x \equiv (i-1)\Delta x + x_\epsilon$, and $y \equiv (j-1)\Delta y + y_\epsilon$, such that $x_\epsilon \in [0, \Delta x]$ (and similarly y_ϵ), we see that periodicity implies that $\mathbf{T}(x,y)$ is equal to $\mathbf{T}(x_\epsilon, y_\epsilon)$. Hence

$$\boldsymbol{F} = \sum_{i,j}\int_{(i-1)\Delta x}^{i\Delta x}\mathrm{d}x_\epsilon\int_{(j-1)\Delta y}^{j\Delta y}\mathrm{d}y_\epsilon \mathbf{T}(x_\epsilon,y_\epsilon)\cdot\hat{n}$$

We observe that the second part in equation above is just the force on the unit cell of the structure ($\boldsymbol{F}^{\mathrm{u.c.}}$), specifically

$$\boldsymbol{F} = \sum_{i,j}\boldsymbol{F}^{\mathrm{u.c}} = \int \mathrm{d}x\mathrm{d}y\, \boldsymbol{P}^{\mathrm{u.c}}$$

with $\boldsymbol{P}^{u.c.} = \boldsymbol{F}^{u.c.}/(\Delta x \Delta y)$ being the pressure on the unit cell. In this analysis, we assumed periodic boundary conditions for the electromagnetic field at the unit cell boundaries. We apply the same approach for torque evaluation. For example,

$$Q_z = \int_{\partial S}(xT_y - yT_x)\,\mathrm{d}x\mathrm{d}y$$

such that

$$Q_z = \sum_{i,j} \int_{u.c.} [((i-1)\Delta x + x_\epsilon)T_y - ((j-1)\Delta y + y_\epsilon)T_x]$$
$$= \sum_{i,j} \left[(i-1)\Delta x \int_{u.c.} T_y - (j-1)\Delta y \int_{u.c.} T_x + \int_{u.c.} (x_\epsilon T_y - y_\epsilon T_x) \right]$$

where $\int_{u.c.}$ denotes the integral over the unit cell. The expression above then becomes

$$Q_z = \sum_{i,j} \left[(i-1)\Delta x F_y^{u.c.} - (j-1)\Delta y F_x^{u.c.} \right] + \sum_{i,j} Q_z^{u.c.}$$

where $F^{u.c.}, Q^{u.c.}$ denote the force/torque on the unit cell. In this expression, we note a contribution to the torque generated by the radiation pressure force (and its corresponding arm), as well as the sum of the unit-cell torques. To get the relevant scaling, we assume the macroscopic structure boundaries along x, y extend from $[-D/2, D/2]$. Converting the sum into an integral, we recover

$$Q_z \sim \iint_{-D/2}^{D/2} \mathrm{d}x\mathrm{d}y \, [xP_y - yP_x] + \iint_{-D/2}^{D/2} \mathrm{d}x\mathrm{d}y q_z^{u.c.}$$

where $q_z^{u.c.} \equiv Q_z^{u.c.}/(\Delta x \Delta y)$. With a change of variables $x' = x/D$ (and similarly for y'), it follows

$$Q_z \sim D^3 \iint_{-1/2}^{1/2} \mathrm{d}x'\mathrm{d}y' \, [x'P_y - y'P_x] + D^2 \iint_{-1/2}^{1/2} \mathrm{d}x'\mathrm{d}y' q_z^{u.c.}$$

From here, we observe that the radiation pressure force contribution to the torque dominates at macroscopic structure sizes ($D \gg \Delta x, \Delta y$). We derive similar expressions for the x, y contributions to the torque, to obtain:

$$Q_x \sim D^3 \iint_{-1/2}^{1/2} \mathrm{d}x'\mathrm{d}y'[y'P_z - z'P_y] + D^2 \iint_{-1/2}^{1/2} \mathrm{d}x'\mathrm{d}y' q_x^{u.c.}$$
$$Q_y \sim D^3 \iint_{-1/2}^{1/2} \mathrm{d}x'\mathrm{d}y'[-x'P_z + z'P_x] + D^2 \iint_{-1/2}^{1/2} \mathrm{d}x'\mathrm{d}y' q_y^{u.c.}$$

In our subsequent analysis, we assume the first ($\propto D^3$) terms in the torque expressions are the dominant ones.

III. METASURFACE ELEMENT FOR PASSIVE STABILIZATION (MEPS)

The change of momentum $\Delta\vec{p}$ of incident light can be expressed as:

$$\Delta\vec{p} = \vec{p}_R + \vec{p}_T - \vec{p}_0$$

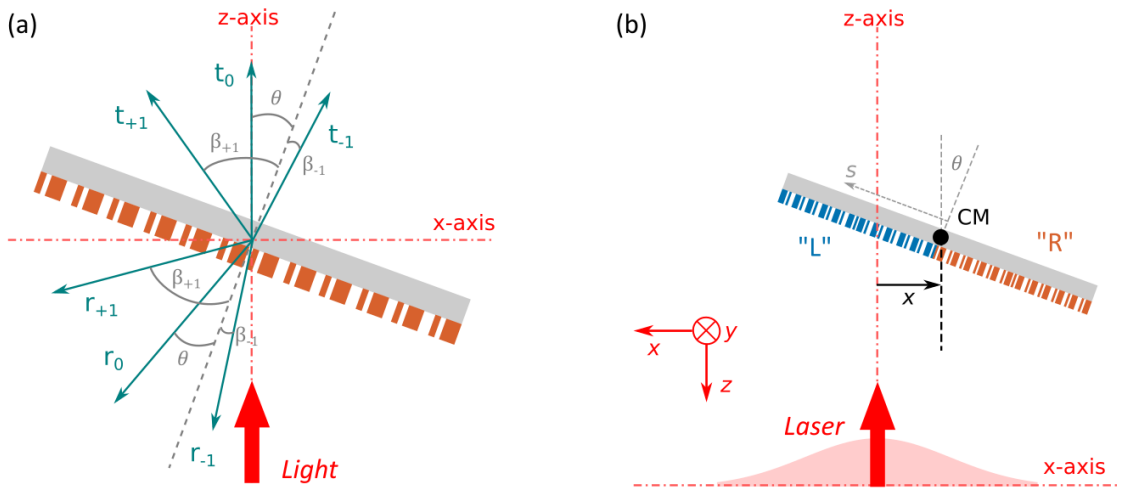

FIG. S3. (a) A diffracting metasurface can generally refract incident light in multiple directions. By collecting the relevant diffracting orders, the total light-induced pressure can be determined. (b) A metasurface element for passive stabilization (MEPS) that comprises two such diffracting metasurfaces placed side-by-side, where one is flipped to achieve mirror symmetry with respect to the center of mass (CM). Here, the two parts are "L" (blue) and "R" (red).

where subscripts R, T, and 0 corresponds to reflected, transmitted, and incident light, respectively. For the choice of materials and the operating wavelength regime analyzed in this work, the absorption in the structure will be negligible. Since the exerted force is proportional to the change of momentum $\boldsymbol{F} = -\frac{\Delta\vec{p}}{\Delta t}$, and $\Delta p = \frac{I}{c}\Delta t$ (where I is the intensity) we can express the total pressure ($\boldsymbol{p}$) that light exerts on the structure. The pressure depends on the tilt angle (θ) and can be decomposed into its x- and z- components, as

$$p_x(\theta) = -\frac{I_0}{c}\left[\sum_{m\neq 0} t_m \sin(\beta_m - \theta) + \left(r_0 \sin(2\theta) + \sum_{m\neq 0} r_m \sin(\beta_m + \theta)\right)\right] \tag{S1}$$

$$p_z(\theta) = -\frac{I_0}{c}\left[-t_0 + \sum_{m\neq 0} -t_m \cos(\beta_m - \theta) + \left(r_0 \cos(2\theta) + \sum_{m\neq 0} r_m \cos(\beta_m + \theta)\right) + 1\right]$$

where r and t correspond to the reflection and transmission coefficients of the relevant orders (and depend on the tilt angle θ). Given the pressure on the unit cell of a uniform structure (Fig. S3a), we can calculate the total force and torque on a MEPS that comprises two such components placed side-by-side, with mirror symmetry with respect to the center of mass (Fig. S3b). When the center of mass is displaced by x from the beam axis and the structure

tilted by angle θ, we write the total force on the MEPS as

$$F_{x,z}(x,\theta) = F^L_{x,z}(x,\theta) + F^R_{x,z}(x,\theta) \tag{S2}$$

where the superscripts L and R correspond to the respective halves of the MEPS (shown colored in blue and red in Fig. S3b). Because the two halves consist of mirror-image unit cells, the following relations apply:

$$\begin{aligned} F^L_z(\pm\theta) &= F^R_z(\mp\theta) \\ F^L_x(\pm\theta) &= -F^R_x(\mp\theta) \end{aligned} \tag{S3}$$

Assuming a Gaussian incident beam with intensity $I(x) = I_0 e^{-2x^2/w^2}$ (where w is the beam waist), we can express the forces (per unit depth in the y-direction) as

$$\begin{aligned} F^L_{x,z}(x,\theta) &= \int_0^{D/2} \mathrm{d}s \cos(\theta) p^L_{x,z}(\theta) e^{-2(x+s\cos(\theta))^2/w^2} \\ F^R_{x,z}(x,\theta) &= \int_0^{D/2} \mathrm{d}s \cos(\theta) p^R_{x,z}(\theta) e^{-2(x-s\cos(\theta))^2/w^2} \end{aligned} \tag{S4}$$

where D is the diameter, and the expressions for $p^{L,R}_{x,z}(\theta)$ are determined from Eqs. (S1). Similarly, we can express the torque on the MEPS (per unit depth in the y-direction) as

$$\begin{aligned} \tau_y(x,\theta) = &\int_0^{D/2} \mathrm{d}s \cos(\theta) s \left[-\sin(\theta) p^L_x(\theta) - \cos(\theta) p^L_z(\theta) \right] e^{-2(x+s\cos(\theta))^2/w^2} + \\ &+ \mathrm{d}s \cos(\theta) s \left[+\sin(\theta) p^R_x(\theta) + \cos(\theta) p^R_z(\theta) \right] e^{-2(x-s\cos(\theta))^2/w^2} \end{aligned} \tag{S5}$$

In this analysis we assume $w \gg \mathrm{d}s$, such that the beam intensity is approximately constant across the $\mathrm{d}s$ element; furthermore, we assume $\mathrm{d}s \gg d$ (where d is the period), such that the element $\mathrm{d}s$ contains a large number of unit cells to be considered as a periodic array itself.

In Fig. (S4), we compare the numerical values for the normalized force/torque from Fig. 2 of the main text obtained with two distinct approaches. Solid lines show the values calculated using the photon momentum balance approach from Eqs. (S2-S5). On the other hand, crosses show the same values calculated via the Maxwell stress tensor along the bounding box that encloses the unit cell. Both sets of calculations are performed using the finite-element-method solver COMSOL Multiphysics. We observe excellent correspondence between the two approaches.

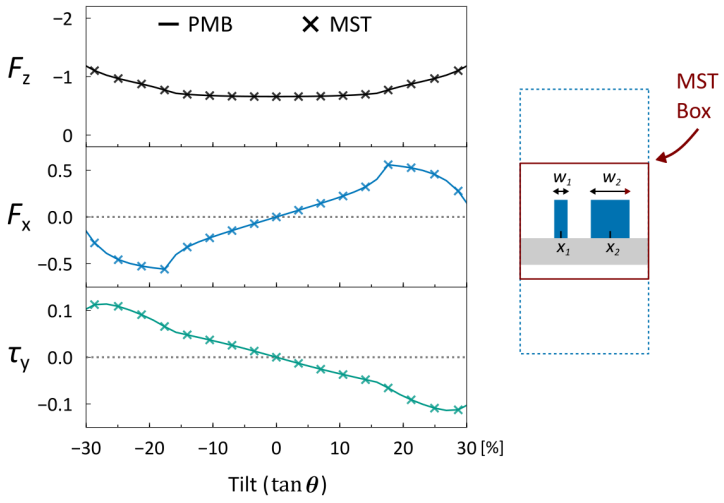

FIG. S4. Comparing the force/torque obtained by photon momentum balance (PMB) from Eqs. (S2-S5), and the Maxwell stress tensor (MST). For the latter case, the stress tensor is integrated around a bounding box that encloses the unit cell (shown on the right). The two methods show excellent agreement.

To highlight the most important aspects of the dynamics, we now restrict our analysis to the x-z plane (where the only rotation considered is the one about the y-axis), and assume no z-dependence of the light intensity along the structure. From the expressions for the net force and torque, we can write the coupled equations of motion

$$\begin{aligned} m\frac{\mathrm{d}^2 z}{\mathrm{d}t^2} &= F_z(x,\theta) - mg \\ m\frac{\mathrm{d}^2 x}{\mathrm{d}t^2} &= F_x(x,\theta) \\ I\frac{\mathrm{d}^2 \theta}{\mathrm{d}t^2} &= \tau_y(x,\theta) \end{aligned} \tag{S6}$$

where m is the total mass, and $I = \gamma m D^2$ is the moment of inertia with respect to the center of mass. In general, γ is a scalar that depends on the macroscopic shape of the MEPS. Because our analysis focuses on the dynamics in the x-z plane, we assume uniformity in the y-direction, as well as uniform mass distribution along the structure: hence, $\gamma = 1/12$ (for rotation around the y-axis), and m is the mass of the MEPS per unit depth in the y-direction.

It is convenient to express all lengths in this problem in the units of the MEPS diameter D. To that effect, we adopt the convention of primed variables, where $l' \equiv l/D$ for any

length variable l. With this in mind, the expressions for the force and the torque (S6) become

$$F_z(x,\theta) = \frac{I_0 D}{c}\int_0^{1/2} \mathrm{d}s' \cos(\theta)\left[p_z'^L(\theta)e^{-2(x'+s'\cos(\theta))^2/w'^2} + p_z'^R(\theta)e^{-2(x'-s'\cos(\theta))^2/w'^2}\right]$$

$$F_x(x,\theta) = \frac{I_0 D}{c}\int_0^{1/2} \mathrm{d}s' \cos(\theta)\left[p_x'^L(\theta)e^{-2(x'+s'\cos(\theta))^2/w'^2} + p_x'^R(\theta)e^{-2(x'-s'\cos(\theta))^2/w'^2}\right]$$

$$\tau_y(x,\theta) = \frac{I_0 D^2}{c}\int_0^{1/2} \mathrm{d}s' \cos(\theta)s'\left[-\sin(\theta)p_x'^L(\theta) - \cos(\theta)p_z'^L(\theta)\right]e^{-2(x'+s'\cos(\theta))^2/w'^2} +$$
$$+ \mathrm{d}s' \cos(\theta)s'\left[\sin(\theta)p_x'^R(\theta) + \cos(\theta)p_z'^R(\theta)\right]e^{-2(x'-s'\cos(\theta))^2/w'^2}$$

where we define the normalized (unitless) pressure $p'_{x,z} \equiv (c/I_0)p_{x,z}$ (S1), and assume the radiation pressure dominates over the weight. Similarly, the equations of motion (S6) transform to

$$\frac{\mathrm{d}^2 z'}{\mathrm{d}t'^2} = \int_0^{1/2} \mathrm{d}s' \cos(\theta)\left[p_z'^L(\theta)e^{-2(x'+s'\cos(\theta))^2/w'^2} + p_z'^R(\theta)e^{-2(x'-s'\cos(\theta))^2/w'^2}\right] = f_{z'}(x',\theta)$$

$$\frac{\mathrm{d}^2 x'}{\mathrm{d}t'^2} = \int_0^{1/2} \mathrm{d}s' \cos(\theta)\left[p_x'^L(\theta)e^{-2(x'+s'\cos(\theta))^2/w'^2} + p_x'^R(\theta)e^{-2(x'-s'\cos(\theta))^2/w'^2}\right] = f_{x'}(x',\theta)$$

$$\frac{\mathrm{d}^2 \theta}{\mathrm{d}t'^2} = \frac{1}{\gamma}\int_0^{1/2} \mathrm{d}s' \cos(\theta)s'\left[-\sin(\theta)p_x'^L(\theta) - \cos(\theta)p_z'^L(\theta)\right]e^{-2(x'+s'\cos(\theta))^2/w'^2} +$$
$$+ \mathrm{d}s' \cos(\theta)s'\left[\sin(\theta)p_x'^R(\theta) + \cos(\theta)p_z'^R(\theta)\right]e^{-2(x'-s'\cos(\theta))^2/w'^2} = f_\theta(x',\theta)$$

where we introduce the normalized time $t' \equiv t/\sqrt{mc/I_0}$ and define the expressions on the right hand side to be $f_{z'}$, $f_{x'}$, f_θ, respectively. Note that the quantity mc/I_0 has units of $[s^2]$, since we assume m is the mass per unit depth in the y-direction. Consequently the scaled equations of motion are dimensionless. For the remainder of this section, we drop the primed notation for dimensionless variables.

In the equations of motion, we observe that rotation and translation are coupled. For this transverse motion, we write the equations of the system in vector form $\mathrm{d}\mathbf{u}/\mathrm{d}t = \mathbf{f}(\mathbf{u})$ where $\mathbf{u} = (x, \theta, v, \omega)^T$ and $\mathbf{f} = (v, \omega, f_x, f_\theta)^T$. From the expressions for $f_{x,z}$, we observe that the origin $\mathbf{u}_0 = 0$, is an equilibrium point of the system, since $\mathbf{f}(\mathbf{u}_0) = 0$. We calculate the Jacobian matrix $\mathbf{f}'(\mathbf{u}_0)$ as

$$\mathbf{f}'(\mathbf{u}_0) = \left[\begin{matrix} 0 & 0 & 1 & 0 \\ 0 & 0 & 0 & 1 \\ \partial f_x/\partial x & \partial f_x/\partial\theta & 0 & 0 \\ \partial f_\theta/\partial x & \partial f_\theta/\partial\theta & 0 & 0 \end{matrix}\right]\Bigg|_{\mathbf{u}_0} \equiv \left[\begin{matrix} 0 & 0 & 1 & 0 \\ 0 & 0 & 0 & 1 \\ f_{xx} & f_{x\theta} & 0 & 0 \\ f_{\theta x} & f_{\theta\theta} & 0 & 0 \end{matrix}\right]\Bigg|_{\mathbf{u}_0} \tag{S7}$$

where we use the shorthand $f_{ij} \equiv \partial f_i / \partial j$, for convenience. The four eigenvalues Λ_{1-4} of the Jacobian are given by

$$\Lambda_{1-4} = \pm \frac{1}{\sqrt{2}} \sqrt{f_{xx} + f_{\theta\theta} \pm \sqrt{(f_{xx} - f_{\theta\theta})^2 + 4 f_{\theta x} f_{x\theta}}}$$

We seek the condition where no eigenvalue has a positive real part. Due to the symmetry of the expression above (and the lack of any damping terms in this particular treatment), this is equivalent to requiring eigenvalues be purely imaginary (marginally stable). For this to be true, the following three conditions $c_{1,2,3}$ need to be satisfied:

$$\begin{aligned} c_1 &\equiv (f_{xx} - f_{\theta\theta})^2 + 4 f_{\theta x} f_{x\theta} > 0 \\ c_2 &\equiv -(f_{xx} + f_{\theta\theta}) > 0 \\ c_3 &\equiv f_{xx} f_{\theta\theta} - f_{\theta x} f_{x\theta} > 0 \end{aligned} \tag{S8}$$

For the structure shown in Fig. 2 of the main text, we numerically evaluate the gradients to obtain: $\partial f_x / \partial x = -0.0853$, $\partial f_x / \partial \theta = 2.05$, $\partial f_\theta / \partial x = -0.638$, $\partial f_\theta / \partial \theta = -4.54$, all evaluated at the origin $\mathbf{u}_0$. By inspection, we deduce the eigenvalues of the Jacobian matrix $\mathbf{f}'(\mathbf{u}_0)$ to be $\Lambda_{1,3} \approx \pm 2.05i$, and $\Lambda_{2,4} \approx \pm 0.63i$. The imaginary nature of the eigenvalues also points to oscillations in the system with relevant frequencies $\Omega_i = \mathrm{Im}(\Lambda_i)$. Physically, this corresponds to first order to a structure oscillating around the center axis of the beam, while accelerating in the z-direction. Fig. S5 compares the actual and the fitted values of $f_{x,\theta}$.

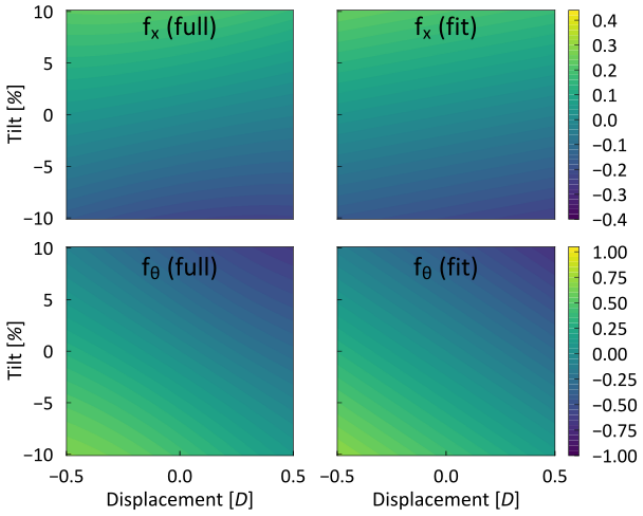

FIG. S5. Comparison between the actual and the fitted values of $f_{x,\theta}$.

Accurately identifying the boundaries of the basin of attraction for this 4-parameter, coupled, non-linear problem is non-trivial. To get some sense of the subset of allowable parameters that give rise to bounded dynamics over analyzed timescales, here we perform a sweep over a range of both initial displacements and tilts. As one example, we set the initial displacement to be $\in [-0.5D, 0.5D]$ and tilt $\in [-10\%, 10\%]$, with respective steps of $0.1D$ and 2%, for a total of 121 dynamical simulations. Each dynamical simulation is evolved up to time $t = 10^3 t_0$ (where the normalized time step is $t_0 = \sqrt{m_l c/I_0}$), and we observe stable dynamics with bounded amplitudes of motion.

We repeat this sweep while adding a small amount of white noise (1% deviation) to the light intensity as a potential variation in the laser power. Over the analyzed time-scales ($\sim 10^3 t_0$), we observe similar bounded dynamics. We remark that the impact of such noise on self-stabilizing properties of nanophotonic structures is generally complex. It depends on many factors, including the intensity and spectral profile of the noise as well as the shape and power of the incident light beam, and affects the spatial and temporal scales for bounded dynamics [37].

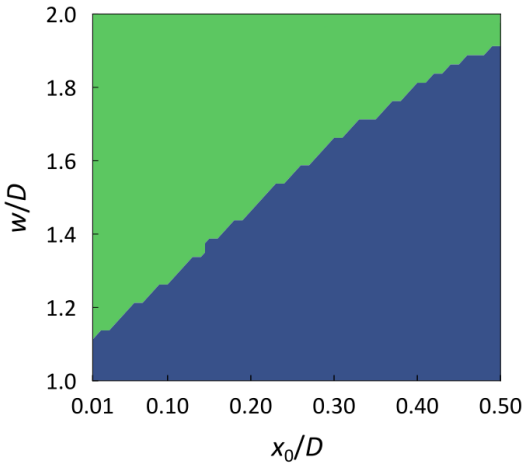

FIG. S6. Numerically evolving dynamical equations of motion for different values of the beam widght (w) and the initial transverse displacement of the structure (x_0). Here, D is the diameter of the structure. We assume the structure is not tilted initially. Area in green correspons to tilt not exceeding 20%.

As discussed in the main text, self-restoring behavior of the structure is influenced by its size relative to the width of the illuminating beam. In Fig. S6, we show the map of the

beam width (w) and the initial displacement (x_0) needed to ensure the structure will not exceed a set tilt $\tan\theta_S$. Here, we choose set tilt of $\sim$20% to be approximately consistent with the domain of linear behavior for the force and the torque (Fig. 2c).

We discuss how the introduction of damping can assist with asymptotic stability of motion around the beam axis. Without specifying a particular physical damping mechanism, we assume a linear dependence of damping force on velocity $g_x = \mu_t v_x$, and the damping torque on angular velocity $g_\theta = \mu_r \omega$ (similar to e.g. Stokes drag). Here, coefficients μ_t, μ_r (for translational and rotational motion, respectively) are assumed to be appropriately scaled to make $g_{x,\theta}$ consistent with the normalized forces and torques in (S7).

Adding these damping terms to the previously evaluated Jacobian elements for our structure, we sweep the values of $\mu_{t,r}$, to find the paramter space where the dynamics is asymptotically stable (i.e. every eigenvalue has strictly negative real part). This is shown in Fig. S7. In addition to the expected condition $\mu_{t,r} < 0$, we also find that the domain for asymptotic stability appears to be bounded on the top, and to the right. The bounding relationships can be numerically approximated as $\mu_t < 0.07\mu_r$ (top) and $\mu_t > 9.5\mu_r - 141\mu_r^2$ (right), and point to considerations for incorporating damping into this system.

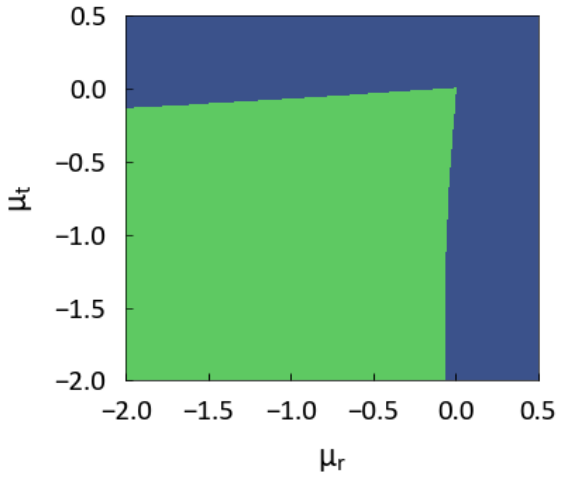

FIG. S7. Parameter space corresponding to asymptotic stability of the beam axis (green) for a range of damping coefficients for translation (μ_t) and rotation (μ_r).

IV. COMPOSITE STRUCTURE: EQUATIONS OF MOTION

We assume the position and the orientation of the composite, rigid-body structure is described by its center of mass coordinates $\boldsymbol{r} = (x, y, z)$, and its orientation by the three Euler angles $\boldsymbol{\alpha} = (\psi, \theta, \phi)$. Here, we use the 1-2-3 (also known as x-y'-z'') convention of rotations in the following sequence: (1) rotation about the x-axis by angle ϕ; (2) rotation about the new position of the y-axis by angle θ; (3) rotation about the new position of the z-axis by angle ψ. For this set of transformations, the direction cosine matrix $\mathbf{H}_I^B$ is [2]

$$\mathbf{H}_I^B(\boldsymbol{\alpha}) = \begin{bmatrix} \cos\psi\cos\theta & \cos\psi\sin\theta\sin\phi + \sin\psi\cos\phi & -\cos\psi\sin\theta\cos\phi + \sin\psi\sin\phi \\ -\sin\psi\cos\theta & -\sin\psi\sin\theta\sin\phi + \cos\psi\cos\phi & \sin\psi\sin\theta\cos\phi + \cos\psi\sin\phi \\ \sin\theta & -\cos\theta\sin\phi & \cos\theta\cos\phi \end{bmatrix}$$

We express the equations for kinematics and dynamics as [2]:

$$\begin{aligned} \dot{\boldsymbol{r}} &= \boldsymbol{v} \\ \dot{\boldsymbol{\alpha}} &= \mathbf{L}_B^I \boldsymbol{\omega} \\ \dot{\boldsymbol{v}} &= \frac{1}{m}\boldsymbol{F}(\boldsymbol{r}, \boldsymbol{\alpha}) - \boldsymbol{g} \\ \dot{\boldsymbol{\omega}} &= \mathbf{I}^{-1}\left[-\boldsymbol{\omega} \times \mathbf{I}\boldsymbol{\omega} + \boldsymbol{\tau}(\boldsymbol{r}, \boldsymbol{\alpha})\right] \end{aligned}$$

where the translational quantities $(\boldsymbol{r}, \boldsymbol{v}, \boldsymbol{F})$ are expressed in the light beam frame, and

$$\dot{\boldsymbol{\alpha}} = \begin{bmatrix} \dot{\psi} \\ \dot{\theta} \\ \dot{\phi} \end{bmatrix} = \begin{bmatrix} -\cos\psi\tan\theta & \sin\psi\tan\theta & 1 \\ \sin\psi & \cos\psi & 0 \\ \cos\psi\sec\theta & -\sin\psi\sec\theta & 0 \end{bmatrix} \begin{bmatrix} \omega_x \\ \omega_y \\ \omega_z \end{bmatrix} = \mathbf{L}_B^I \boldsymbol{\omega}$$

relates the time derivative of the Euler angles to the components of the angular velocity. Assuming the moment of inertia tensor is diagonal, with I_x, I_y, I_z the principal moments of inertia, we can simplify the Euler equation above to obtain:

$$\begin{aligned} I_x\dot{\omega}_x &= \tau_x - (I_z - I_y)\omega_y\omega_z \\ I_y\dot{\omega}_y &= \tau_y - (I_x - I_z)\omega_x\omega_z \\ I_z\dot{\omega}_z &= \tau_z - (I_y - I_x)\omega_x\omega_y \end{aligned}$$

As before, we focus on self-restoring behavior transverse to the light beam. We assume the beam depth of focus is large enough that the variation of the beam intensity along

the z-axis is negligible, and ignore the gravitational term. With this in mind, the motion along the z-axis is independent of the coupled translation (along x-y) and rotation (ψ, θ, ϕ), and we write the ten-dimensional state vector as $\mathbf{u} = (\boldsymbol{r}, \boldsymbol{\alpha}, \boldsymbol{v}, \boldsymbol{\omega})$, where $\boldsymbol{r} = (x_c, y_c)$, and $\boldsymbol{v} = (v_x, v_y)$ are the position and the velocity of the center of mass. Near the origin $\mathbf{u} = 0$, we can linearize to obtain $\dot{\boldsymbol{\alpha}} \approx \boldsymbol{\omega}$ and $\dot{\boldsymbol{\omega}} \approx \mathbf{I}^{-1}\boldsymbol{\tau}$.

The schematic of a proof-of-concept structure illustrated in Fig. 4 is shown in more detail in Fig. S8. We assume two different building-block designs, "a" shown in blue and "b" shown in orange, are used to define six separate regions of the structure (1-6 as shown in Fig. S8). The proof-of-concept structure has an overall diameter of D along both the x and the y axes, and the boundary between region "a" and region "b" is at position $\pm s_x D$, where parameter $s_x \in [0, \frac{1}{2}]$. Given the order of the Euler angle rotations, when the composite

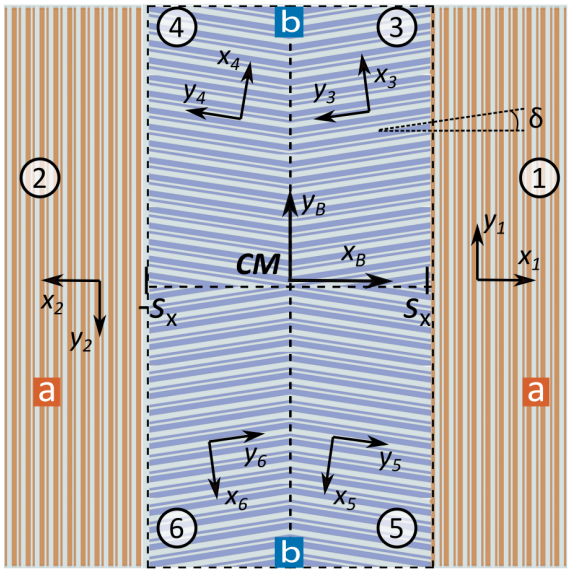

FIG. S8. Top view of the composite structure from Fig. 4 of the main text that combines two MEPS elements, one for region "a" and the other for region "b". The structure has an overall diameter D along both the x and the y axis. The elements in structure "b" are rotated by angle δ to provide yaw (ψ) torque. Parameters of the structure are given in Methods.

structure is oriented at an angle $\boldsymbol{\alpha} = (\psi, \theta, \phi)$, we can transform the polarization vector into each of the $j = 1, 2, \ldots 6$ regions as:

$$\mathbf{E}_j = \mathbf{H}_I^B(\psi + \beta_j, \theta, \phi)\mathbf{E}_I$$

where $\beta_{1,2,...6} = 0, \pi, \frac{\pi}{2}+\delta, \frac{\pi}{2}-\delta, \frac{3\pi}{2}-\delta, \frac{3\pi}{2}+\delta$. Similar relationship applies to transforming the $\mathbf{k}$ vector. In the reference frame of the laser, we assume the incident beam of light is polarized along the y-axis, $\mathbf{E}_I = E_0(0,1,0)$, and propagates along the negative z-axis, $\mathbf{k}_I = k_0(0,0,-1)$.

The beam of light induces pressure on region j, which we denote as $\boldsymbol{p}'_j$ in its own frame. Relative to body coordinates (x_b, y_b), this pressure can be expressed as $\boldsymbol{p}_j = \boldsymbol{C}(\beta_j)\boldsymbol{p}'_j$, where

$$\boldsymbol{C}(\beta_j) = \begin{bmatrix} \cos\beta_j & -\sin\beta_j & 0 \\ \sin\beta_j & \cos\beta_j & 0 \\ 0 & 0 & 1 \end{bmatrix}$$

Given these, we can, per our earlier derivation, calculate the optically induced force and torque on each region as a function of the orientation ($\boldsymbol{\alpha}$) and the lateral position of the center of mass (x_c, y_c) as:

$$\boldsymbol{F}_j(x_c, y_c, \boldsymbol{\alpha}) = \eta \iint \mathrm{d}x_b \mathrm{d}y_b \;\; \boldsymbol{p}_j(\boldsymbol{\alpha}) \; I(\mathbf{r}(x_c, y_c, x_b, y_b))$$

and

$$\boldsymbol{\tau}_j(x_c, y_c, \boldsymbol{\alpha}) = \eta \iint \mathrm{d}x_b \mathrm{d}y_b \;\; (x_b, y_b, 0)^T \times \boldsymbol{p}_j(\boldsymbol{\alpha}) \; I(\mathbf{r}(x_c, y_c, x_b, y_b))$$

where $\eta = \cos(\theta)\cos(\phi)$ accounts for the projected area, and $I(\mathbf{r}) = (I_0/c)\exp(-2\left|\mathbf{r}\right|^2/w^2)$ is the spatial variation of the beam intensity. Note that $\boldsymbol{p}_j(\boldsymbol{\alpha})$ are different for different j, so multiple EM simulations are needed for a single orientation $\boldsymbol{\alpha}$. An element at position x_b, y_b (in the body frame) has beam frame transverse coordinates given by:

$$\mathbf{r}(x_c, y_c, x_b, y_b) = \begin{bmatrix} x_c \\ y_c \\ 0 \end{bmatrix} + \mathbf{H}_B^I(\boldsymbol{\alpha}) \begin{bmatrix} x_b \\ y_b \\ 0 \end{bmatrix}$$

Finally, in the equation above, the limits of the double integral correspond to the region boundaries. For example, region 1 spans $[s_x, \frac{1}{2}]D$ and $[-\frac{1}{2}, \frac{1}{2}]D$ along the x and the y axis, respectively. Summing the contributions from each region of the structure and converting to the beam frame, we obtain the total force $\boldsymbol{F} = \sum_j \boldsymbol{F}_j$ and torque $\boldsymbol{\tau} = \sum_j \boldsymbol{\tau}_j$, which are the inputs used in equations for the kinematics and dynamics.

For the structure shown in Fig. (S8), we assume the mass per unit area of regions (a) and (b) is denoted by χ_a and χ_b, respectively. From this, we can express the total mass of

the structure as

$$m = 2\left[\chi_a(1/2 - s_x) + \chi_b s_x\right] D^2$$

where s_x denotes the position of the boundary that separates regions (a) and (b). Similarly, the moments of inertia with respect to the three (body) axes can be calculated

$$\begin{aligned} I_x &= \left[\chi_a(1/2 - s_x) + \chi_b s_x\right] \frac{D^4}{6} \\ I_y &= \left[\frac{\chi_a}{12} + 2(\chi_b - \chi_a)\frac{s_x^3}{3}\right] D^4 \\ I_z &= I_x + I_y \end{aligned}$$

For the case of $s_x = 1/4$ (regions a and b have the same area), expressions above simplify:

$$\begin{aligned} m &= (\chi_a + \chi_b)\frac{D^2}{2} \\ I_x &= (\chi_a + \chi_b)\frac{D^4}{24} \\ I_y &= (7\chi_a + \chi_b)\frac{D^4}{96} \end{aligned}$$

We now derive the expressions for mass-per-unit-area quantities $\chi_{a/b}$. The mass of a unit cell depicted in Fig. 2 can be expressed as

$$m_{\text{u.c.}} = d^2\left[t\rho_s + (w_1 + w_2)h\rho_e\right]$$

where d is the period, ρ_s is the mass density of the substrate layer (silica), and ρ_e the density of the resonating elements (silicon). From here it follows that the mass per unit area χ of such a structure is simply

$$\chi = t\rho_s + (w_1 + w_2)h\rho_e$$

Using the values of $\rho_s \approx 2.2\text{g/cm}^3$ (silica), and $\rho_e \approx 2.3\text{g/cm}^3$ (silicon), as well as the design parameters $(t, h, w_{1,2})$, we get the ratio of the area densities, namely

$$\frac{\chi_a}{\chi_b} \approx 1.12$$

Substituting these above, we get the moments of inertia about the principal axes to be $I_x = \frac{1}{12}mD^2$, $I_y \approx \frac{1.04}{12}mD^2$, and $I_z = I_x + I_y \approx \frac{2.04}{12}mD^2$.

Once we know the total force and torque we can, as before, make the equations of motion dimensionless. We introduce the dimensionless quantities for the position coordinate $x' \equiv x/D$ (similar for y', z') to introduce normalized force ($f_{x,y,z}$) and torque ($f_{\phi,\theta,\psi}$) as

$$F_{x,y,z} = \frac{I_0 D^2}{c} f_{x,y,z} \quad \text{and} \quad \tau_{x,y,z} = \frac{I_0 D^3}{c} f_{\phi,\theta,\psi}$$

as well as normalized time $t' \equiv t/\sqrt{mc/I_0 D}$. As before, we can express the time-evolution of the system as $\mathrm{d}\mathbf{u}/\mathrm{d}t = \mathbf{f}(\mathbf{u})$, where $\mathbf{u} = (\boldsymbol{r}, \boldsymbol{\alpha}, \boldsymbol{v}, \boldsymbol{\omega})$ is the state vector. This set of differential equations is numerically evolved in time to compute the dynamics of the system (in the propulsion regime, where the radiation pressure force dominates over the weight).

---

[1] Jackson, J. *Classical Electrodynamics*; John Wiley & Sons, New York, 1999.

[2] Hughes, P. C. *Spacecraft Attitude Dynamics*; Dover Publications, Mineola, N.Y. 11501, 2004.